GSA Data Repository 201793

Pore fluids in Dead Sea sediment core reveal linear response of lake chemistry to global climate changes

Authors: Elan J. Levy, Mordechai Stein, Boaz Lazar, Ittai Gavrieli, Yoseph Yechieli, and Orit Sivan

<u>DR 1</u>: Determining conservativeness of Br^- and Mg^{2+} in pore fluids

Regression analysis was employed to assess the magnitude of conservativeness for Br^- and Mg^{2+} (DR Fig. 1B and 1C) in all pore fluid samples. This was carried out by plotting the relative degree of evaporation (D.E), or molal concentrations ($mol{\bullet}Kg(H_2O)^{-1}$) normalized to Dead Sea concentrations (Eq.1), against each other (i.e. $D.E._{Br}$ vs. $D.E._{Mg}$; DR Fig. 2). Assuming a relatively stable inventory of Br^- and Mg^{2+} (chemical species *i*) in the deep lake over the past 220 kyrs, the degree of evaporation should be approximate to the ratio of H_2O (kg) in the modern Dead Sea, relative to pore fluids H_2O (kg):

$$D.E._i = \frac{[C_i]}{[C_i]_{Dead\ Sea}} \sim \frac{H_2O_{Dead\ Sea}}{H_2O_{Pore\ fluid}} \qquad (1)$$

The plot yields values along a linear trend of y= x, as should be expected for conservative ions (DR Fig. 2). 95% of values fall within a confidence interval of y = x ±0.14. Data points outside the confidence intervals indicate relative non-conservativity and are removed from the pore fluid records (DR table 1). On the plot (DR Fig. 2) a theoretical evaporation/dilution curve of Dead Sea brine was created by incrementally adding or removing H_2O and equilibrating with all the relevant evaporite minerals precipitated in the process. Values were calculated using the Pitzer geochemical dataset in PHREEQC© (Method from Parkhurst and Appelo, 1999, p.209-211). Carnallite ($KMgCl_3{\cdot}6H_2O$) was found to precipitate at a D.E. of ~1.7 ratio, similar to other estimates (Gavrieli et al., 1989; Zilberman-Kron, 2008). Inverting the degree or evaporation yields the degree of dilution ($D.D._i$;Eq. 2) which is the representation used in the manuscript (Fig. 1B) for estimates of relative net water balance changes:

$$D.D._i = \frac{[C_i]_{Dead\ Sea}}{[C_i]} \sim \frac{H_2O_{Pore\ fluid}}{H_2O_{Dead\ Sea}} \qquad (2)$$

<u>DR 2:</u> Depth-age conversion

The published anchor age model for the ICDP core 1A (Torfstein et al., 2015), which is based on the integration of U-Th ages and $\delta^{18}O$ aragonite stratigraphy tied to the $\delta^{18}O_{Benthic}$ LR04 and Soreq Cave $\delta^{18}O$ speleothem curves (see supplementary material *in* Torfstein et al., 2015 for full details), was used to convert depth (mblf) to age (ka) for sediments below >91mblf (older than14.5 ka). To gain high-resolution ages for Holocene sediments, linear interpolation of depths above 91 mblf based on radiocarbon ages of plant material was carried out (Neugebauer et al., 2014). See DR Fig. 1F and Table DR 3 for data points in the compiled age model.

<u>DR 3:</u> Subsurface fluid transport modeling

Pore fluid transport and modification of concentrations was estimated. The ICDP core had been schematically split into four units (I-IV; DR Fig. 1E) depending on sedimentology, magnetic susceptibility, and element scanner data (Neugebauer et al., 2014; DR Fig. 1E). Units I and III are dominated by fine clastic material, gypsum layers, and alternating aragonite and detritus (aad) layers along with some scattered layers of halite close the bottom of unit I, while Units II and IV mostly contain all of the above mentioned but also considerable intermittent layers of halite 'sandwiching' these sediments (DR Fig. 1E). Measured permeability values for Dead Sea halite layers are in the range of 5 X 10^{-13} to 5 X 10^{-15} cm^2 (Weisbrod et al., 2012). A diffusion coefficient for halite species is likely on the scale of 10^{-8} cm^2/s (Ossenbrück et al., 1998), or a factor of 2000-700 times lower than the estimated molecular diffusion coefficients in H_2O (see below). Thus we assume that vertical advection and diffusion through halite layers is negligible.

For sedimentary units I and III, we calculated the dimensionless Peclet number (Pe) for determining advection/diffusion dominated transport. Values of Pe > 1 infer advection dominated transport while Pe << 1 infers diffusion dominated transport. The calculated Pe values for these units are 0.026 and 0.054, similar to a range reported by Adkins et al., (2003) in a marine sediment core. Furthermore, drops in Na/Cl appear to mostly occur at the same interval as halite in the core (see red arrows DR Fig.1E and lithology in Fig. 1F), and the transitions between the four sedimentary units (numbered I-IV; Neugebauer et al., 2014) appear close to the same depths as the major pivot points in the conservative records. Thus, it can be assumed that diffusion is the dominant transport process in the pore fluids over the core and negate vertical advection.

The diffusive transport of conservative Br^- and Mg^{2+} in pore fluids was calculated using a 1D forward diffusion model based on Ficks law (Eq. 3) (Berner, 1980):

$$\frac{\partial \phi [\mathrm{C_{i,z}}]}{\partial \mathrm{t}} = \frac{\partial}{\partial \mathrm{z}} \cdot \left(\mathrm{D_{si}} \phi \frac{\partial [\mathrm{C_{i,z}}]}{\partial \mathrm{z}}\right) - \omega \left(\frac{\partial [\mathrm{C_{i,z}}]}{\partial z}\right) \tag{3}$$

Where: $[C_i]$ is the concentration of conservative species *i* in the pore fluids or the initial concentration conditions for the model (in M), t = time (yrs) from 0 – 220,000, z = layer depth in core from 0 - 455 (m), ϕ is porosity (a dimensionless parameter; see below), D_{si} is the molecular diffusion coefficient for species $_i$ in the sediment including the effects of tortuosity ($m^2 yr^{-1}$), and ω is the rate of deposition or the rate of burial of the layer below the sediment-water interface ($m \cdot yr^{-1}$). A fixed layer coordinate system was used, and assuming no vertical advection relative to the sediment, the term $-\omega\left(\frac{\partial [\mathrm{C_{i,z}}]}{\partial z}\right)$ was removed (Berner, 1980). Furthermore, we assume that $\mathrm{D_{si}}$ is inversely proportional to the molecular diffusion coefficient ($\mathrm{D_0}$) divided by the square of the tortuosity parameter (θ) in the sediment, and that tortuosity converts to porosity using Archie's law using a fitting parameter of *m* =2. Thus the model takes the form of Eq. 4 (below) which was implemented using MATLAB ©:

$$\phi \frac{\partial[C_{i,z}]}{\partial t} = D_{0-DS} \cdot \frac{\partial}{\partial z}\left(\phi^2 \frac{\partial[C_{i,z}]}{\partial z}\right) \quad (4)$$

$D_{0\text{-}DS}$ are the molecular diffusion coefficients in the Dead Sea (DS) and are assumed to be homogenous over the core depth [$m^2 \cdot yr^{-1}$]. D_{0-DS} values were adapted from estimates for D_0 values at infinite dilution in H_2O: either $20.8 \cdot 10^{-6}$ [$cm^2 \cdot sec^{-1}$] or 0.065 [$m^2 \cdot yr^{-1}$] for Br^-, and $7.1 \cdot 10^{-6}$ [$cm^2 \cdot sec^{-1}$] or 0.022 [$m^2 \cdot yr^{-1}$] for Mg^{2+} (25°C) (Cussler, 1997). These were adapted to account for the Dead Sea's high dynamic viscosity: 2.54 cp for Dead Sea (Gat and Shatkay, 1991), in comparison to 0.89 cp for H_2O using the Stokes–Einstein equation. Corrected diffusion coefficients for Dead Sea brine are $D_{0,DS\text{-}Br} = 0.022\ m^2yr^{-1}$ and $D_{0,DS\text{-}Mg} = 0.008\ m^2yr^{-1}$. The porosity, ϕ, for each sedimentary layer (ϕ_z) was estimated based on 31 porosity measurements of detrital sediment found in *ld* and *aad* facies over the core depth (Eq. 5):

$$\phi(z) = 0.13 + (0.55 - 0.13)\exp\left(-\frac{z}{460m}\right)(\pm 0.08) \quad (5)$$

The sedimentation rates in the core based on the anchor age model (Torfstein et al., 2015) were used to estimate $\phi(z)$ at any given time $\phi(z,t)$. For halite layers, a flag setting $\phi = 0$ was set and the model was revised to accommodate these settings. The modeling was carried out in two phases: first, to investigate areas relatively susceptible to diffusive modification of concentrations by setting pre-diffusion concentration prerequisites as the pore fluid concentrations (i.e. $[C_{i,z,t=0}]$ = pore fluid, $[C_{i,z,t=220ka}]$ = ?) (DR Fig. 3A). Depth intervals prone to significant diffusion modification were noted and ignored in the second phase of modeling (i.e. from 320mblf downwards). The second phase involved reconstructing (estimating) pre-diffusion concentrations or concentrations at the sediment-water interface prior to diffusion. Concentrations were estimated usingtrial-and–error ($[C_{i,z,t=0}]$ =? , $[C_{i,z,t=220ka}]$ = pore fluid) until post-diffusion results of the reconstructed concentrations 'fitted' the majority of samples (DR Fig. 3B and 3C). The model was tested by using parameter extremities: $D_{0,DS\text{-}Mg}$ =50% and 150%, and $D_{0,DS\text{-}Mg}$ =300%. This range includes any variability for porosity model extremities (±0.08). Results for D=50% and 150% show repetition within ±5% (DR Fig.3D).

<u>DR 4</u>: Phase analysis of global records and pore fluid conservative records

We investigated the phase relationship between the composite CO_2 record from Antarctic ice cores (Lüthi et al., 2008; Petit et al., 1999; Monin et al., 2001) and the pore fluid Br^- and Mg^{2+} records (Fig. 2 in manuscript for Mg^{2+}). Interpolated data points for pore fluid records (<132 kya - one full interglacial-glacial-interglacialcycle) and CO_2 were calculated at 1kyr intervals and then plotted against each other. The magnitude of phase offset was estimated by sequential phase offset of Br^- and Mg^{2+} backwards in time until the most linear regression was attained (ignoring data points of dilution corresponding to Mediterranean sapropel layers S1 and S5. See manuscript text for explanation). DR table 2 summarises correlation coefficient (r) results.

References

Adkins, J., and Schrag, D., 2003, Reconstructing Last Glacial Maximum bottom water salinities from deep-sea sediment pore fluid profiles: Earth and Planetary Science Letters, v. 216, no. 1-2, p. 109–123.

Berner, R., 1980, Early diagenesis: A theoretical approach: Princeton University Press. p. 241.

Cussler, E.L., 2009, Diffusion: Mass Transfer in Fluid Systems (third edition): Cambridge University Press., Cambridge.

Gat, J. R., and Shatkay, M., 1991, Gas exchange with saline waters: Limnology and Oceanography, v. 36, no. 5, p. 988-997.

Gavrieli, I., Starinsky, A., and Bein, A., 1989, The solubility of halite as a function of temperature in the highly saline Dead Sea brine system: Limnology and Oceanography. v. 34, no. 7, p. 1939-5590.

Lazar, B., Sivan, O., Yechieli, Y., Levy, E.J., Antler, G., Gavrieli, I., and Stein, M ,.2014, Long term freshening of the Dead Sea brine revealed by porewater Cl and d18O in ICDP Dead Sea deep-drill: Earth and Planetary Science Letters, v. 400, p. 94–101, doi: 10 .1016 /j .epsl .2014 .03 .019.

Lüthi, D., et al., 2008, High-resolution carbon dioxide concentration record 650,000-800,000 years before present.: Nature, v. 453, p. 379–382.

Neugebauer, I., et al., 2014, Lithology of the long sediment record recovered by the ICDP Dead Sea Deep Drilling Project (DSDDP): Quaternary Science Reviews, v. 102, p. 149–165.

Martrat, B., Grimalt, J.O., López-Martinez, C., Cacho, I., Sierro, F.J., Flores, J.A., Zahn, R., Canals, M., Curtis, J.H., Hodell, D.A., 2004, Abrupt Temperature Changes in the Western Mediterranean over the Past 250,000 Years: Science, v. 306, p. 1762-1765, doi: 10.1126/science.1101706

Monnin, E., Indermuhle, A., Dallenbach, A., Fluckiger, J., Stauffer, B., Stocker, T.F., Raynaud, D., and Barnola, J.M., 2001. Atmospheric CO2 concentrations over the last glacial termination.: Science, v. 291, p. 112-114.

Ossenbrück, K., Lippmann, J., and Sonntag, C., 1998, Dating very old pore waters in impermeable rocks by noble gas isotopes: Geochimica et Cosmochimica Acta, v.62, no. 18, p. 3041–3045.

Parkhurst, B.D.L., and Appelo, C.A.J., 1999, User's Guide To PHREEQC (version 2) — a Computer Program for Speciation, Batch-reaction, One-dimensional transport, and Inverse Geochemical Calculations: Water-Resources Investigations Report, U.S. Geological Survey, p. 99-4259.

Petit, J.R., et al., 1999. Climate and atmospheric history of the past 420,000 years from the Vostok ice core, Antarctica. Nature v. 399 p. 429-436.

Steinhorn, I., 1985, The disappearance of the long term meromictic stratification of the Dead Sea: Limnology and Oceanography, v. 30, no. 3, p. 451–472, doi: 10.4319/lo.1985.30.3.0451.

Torfstein, A., Goldstein, S.L., Kushnir, Y., Enzel, Y., Haug, G., and Stein, M., 2015, Dead Sea drawdown and monsoonal impacts in the Levant during the last interglacial: Earth and Planetary Science Letters, v. 412, p. 235–244, doi: 10.1016/j.epsl.2014.12.013.

Weisbrod, N., Alon-Mordish, C., Konen, E., and Yechieli, Y., 2012, Dynamic dissolution of halite rock during flow of diluted saline solutions: Geophysical Research Letters, v. 39.

Zilberman-Kron, T., 2008, The source and geochemical evolution of the brines in sinkholes along the western shore of the Dead Sea [M.Sc thesis]: The Hebrew University of Jerusalem, p. 113.

Supplementary figures:

<u>DR Fig 1:</u> Pore fluid profiles, core lithology and age model

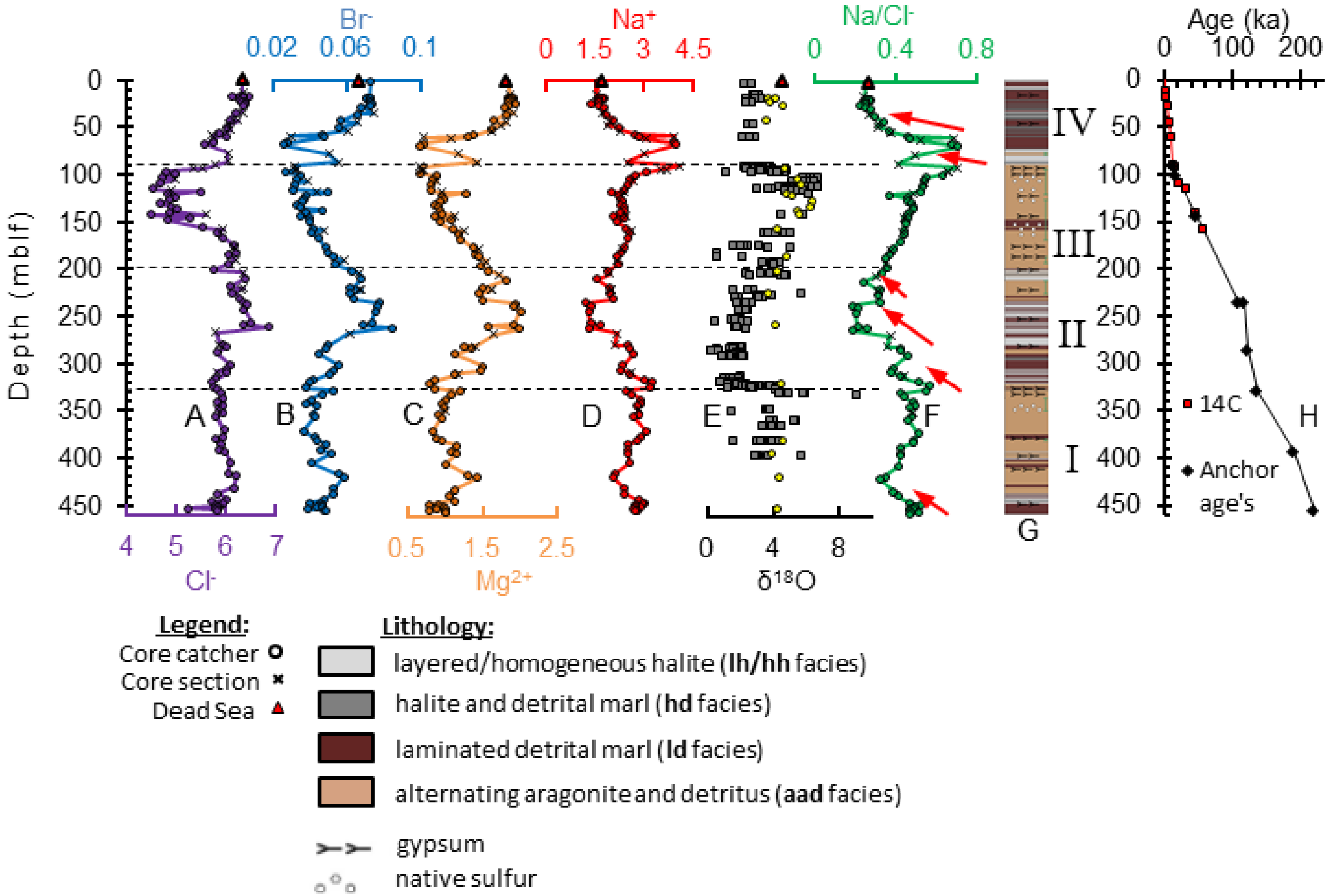

<u>DR Fig. 1:</u> Pore fluid chemical profiles (mol•L^{-1}): (A) Cl^-, (B) Br^-, (C) Mg^{2+}, and (D) Na^+; (E) $\delta^{18}O_{aragonite}$ (‰) in gray squares (Torfstein et al., 2015), $\delta^{18}O_{H2O}$ (‰) in yellow circles (Lazar et al., 2014); (F) Na/Cl (molar ratio; red arrows show decreases in Na/Cl which correlate to halite sequences in the ICDP core); (G) Lithology and sedimentary sections (I-IV) from (Neugebauer et al., 2014); (H) ^{14}C dates from organic material (Neugebauer et al., 2014) and anchor ages (Torfstein et al., 2015). The compiled age model using a combination of these datasets can be found in DR table 3.

<u>DR Fig. 2:</u> D.E.$_{Br}$ vs. D.E.$_{Mg}$.

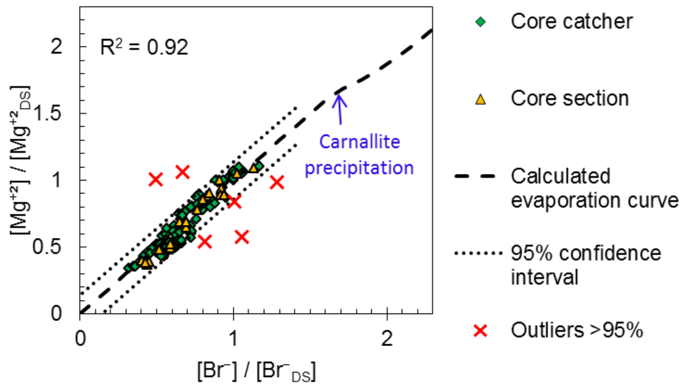

<u>DR Fig. 2:</u> D.E.$_{Br}$ vs. D.E.$_{Mg}$ for core catcher samples (green markers); and core section (yellow markers). ~95% confidence intervals (y = x ±0.14) are marked by the thin black dotted lines. Values outside of the confidence intervals are assumed to be non-conservative (red crosses). On the plot is the theoretical evaporation curve (thick black dashed line) of Dead Sea brine (composition from Steinhorn, 1985) calculated by incremental evaporation/dilution using PHREEQC© software (Parkhurst and Appelo, 1999).

<u>DR Fig. 3:</u> Diffusion models.

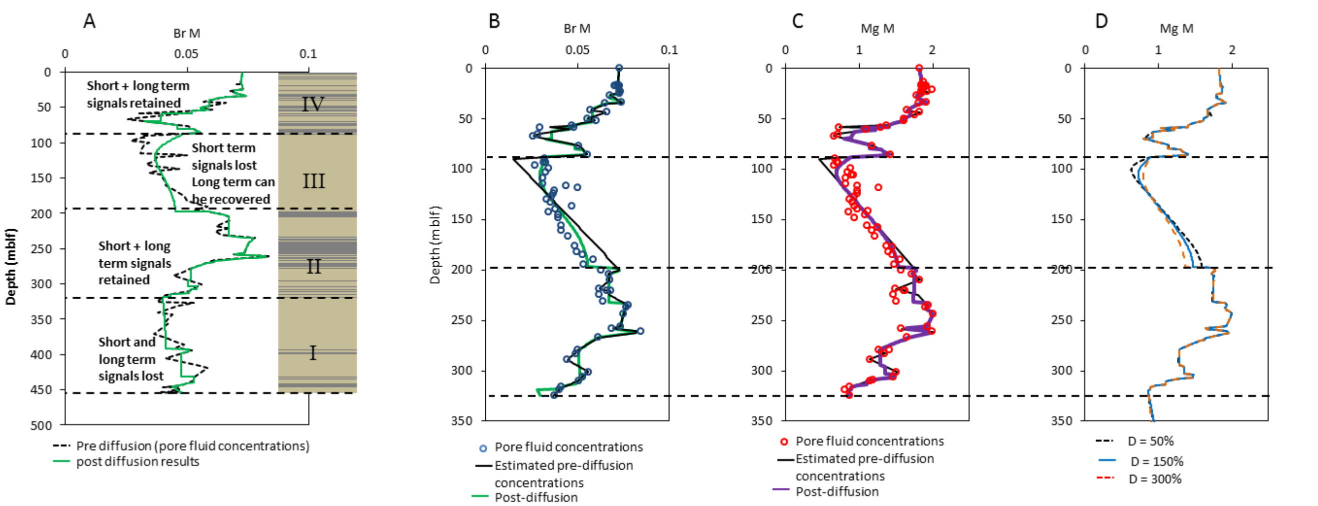

<u>DR Fig. 3:</u> Diffusion modeling results. (A) A model investigating areas susceptible to diffusive reworking of Br^- concentrations; (B) and (C) Estimation of pre diffusion concentrations in the deep lake prior to diffusion for Br^- and Mg^{2+} respectively from 320mblf up; (D) Results of tests of model sensitivity by using diffusion coefficient parameter extremities.

<u>DR Fig. 4:</u> Pore fluid and global climate proxy time series comparison (since 30 ka).

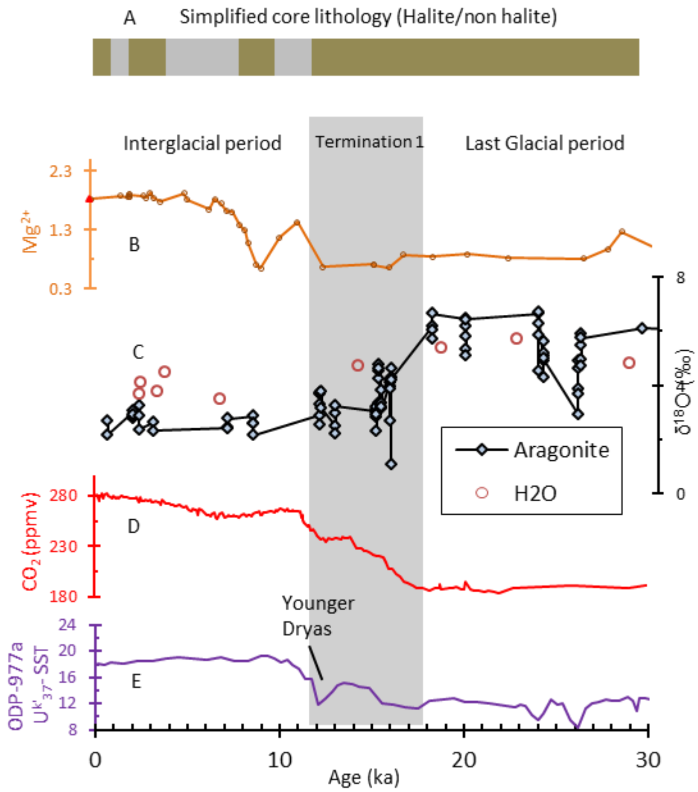

<u>DR Fig 4.</u> (A) Simplified lithology in core 1A (halite/non-halite layers); (B) Pore fluid Mg^{2+} concentration ($mol{\bullet}L^{-1}$). Red triangle is the pre-overturn Dead Sea concentration (Steinhorn, 1985; (C) $\delta^{18}O_{aragonite}$ (‰) from core sediments (Torfstein et al., 2015) and $\delta^{18}O_{H2O}$ from pore fluids (Lazar et al., 2014) (‰); (D) composite CO_2 record (ppmv) (Lüthi et al., 2008) (E) SST based on $U^{k'}_{37}$ alkenone ratio record from marine sediment core ODP977a at the Western Mediterranean Sea (Martrat et al., 2004).

Table DR 1: Pore fluid chemistry (mol•L^{-1}). Samples with notes are removed from the records.

Site-Hole-Shot	Section	CS/CC	Depth (m blf)	Age (ka)	± (kyr)	Age conversion method:	Mg^{2+}	Br^-	Cl-	Na+	Calculated density (Kg/L)	NOTES:
1-A-1	2	CC	0.2	0.0	0.30	14C	1.8251	0.0726	6.3120	1.6272	1.231	
1-A-7	2	CS	14.08	1.6	0.03	14C	1.8720		6.3346	1.5471	1.229	
1-A-7	3	CC	15.3	1.8	0.13	14C	1.8387	0.0360	6.3760	1.6666	1.230	Br / Mg not conservative
1-A-8	3	CC	16.9	2.0	0.13	14C	1.8482	0.0720	6.2649	1.6529	1.228	
1-A-9	1	CC	17.3	2.1	0.13	14C	1.8524	0.0702	6.1406	1.7120	1.226	
1-A-9	1	CC	17.3	2.1	0.13	14C	1.8696	0.0708	6.4410	1.7586	1.235	
1-A-10	1	CC	17.3	2.1	0.13	14C	1.9126	0.0722	6.3412	1.7304	1.232	
1-A-11	2	CC	17.6	2.1	0.13	14C	1.8976	0.0726	6.3580	1.5990	1.231	
1-A-12	1	CS	21.17	2.8	0.03	14C	1.9910	0.0820	6.4483	1.5661	1.234	Artifact?
1-A-12	2	CC	21.6	2.8	0.13	14C	1.8794	0.0727	6.2769	1.5505	1.229	
1-A-13	2	CC	22.5	3.0	0.13	14C	1.8449	0.0726	6.3710	1.6346	1.233	
1-A-13	3	CC	22.6	3.0	0.13	14C	1.9178	0.0721	6.5595	1.7181	1.241	Salt contamination
1-A-14	1	CC	23.6	3.2	0.13	14C	1.9297	0.0733	6.3117	1.4127	1.230	
1-A-16	1	CC	24.7	3.4	0.13	14C	1.8449	0.0726	6.3698	1.6346	1.233	
1-A-17	2	CC	26.8	3.8	0.14	14C	1.7810	0.0675	6.3294	1.7512	1.232	
1-A-20	1	CS	30.74	4.4	0.04	14C	1.9334	0.0484	6.4353	1.6751	1.234	Br /Mg not conservative
1-A-20	3	CC	31.5	4.6	0.14	14C	1.9438	0.0722	6.5582	1.7873	1.239	Salt contamination
1-A-22	1	CS	34.075	5.0	0.04	14C	1.9151	0.0741	6.3433	1.7379	1.233	
1-A-22	2	CC	35.1	5.2	0.15	14C	1.8048	0.0651	6.1956	1.8450	1.227	
1-A-24	3	CC	41.9	6.4	0.15	14C	1.6449	0.0568	6.0754	2.0618	1.223	
1A-25	1	CS	43.51	6.7	0.06	14C	1.8217	0.0659	6.2533	1.9680	1.229	
1-A-25	3	CC	45.9	6.9	0.16	14C	1.8206	0.0640	6.4477	2.1341	1.236	Salt contamination
1-A-26	1	CS	46.71	7.0	0.06	14C	1.7498		6.0635	1.8877	1.223	
1-A-27	2	CC	50.0	7.3	0.16	14C	1.6100	0.0554	6.0230	2.2429	1.223	
1-A-28	1	CS	52.55	7.6	0.06	14C	1.6092	0.0601	6.0917	2.2967	1.225	
1-A-28	3	CC	54.4	7.8	0.16	14C	0.6153	0.0232	5.9990	4.3576	1.234	Salt contamination
1-A-29	2	CC	56.6	8.0	0.16	14C	1.3762	0.0469	5.8859	2.7286	1.221	
1A-30	1	CS	58.66	8.2	0.06	14C	0.7273	0.0296	5.7371	3.9115	1.222	Artifact?
1-A-30	2	CC	59.3	8.3	0.16	14C	1.2919	0.0478	6.0014	2.8248	1.225	
1A-31	1	CS	61.07	8.4	0.06	14C	1.0887		5.7595	3.0311	1.219	
1-A-32	3	CC	65.4	8.9	0.17	14C	0.7053	0.0281	5.7587	3.9017	1.221	
1-A-33	3	CC	67.4	9.1	0.17	14C	0.6560	0.0257	5.5705	3.9303	1.216	
1-A-38	1	CS	76.76	10.1	0.09	14C	1.1749	0.0505	6.0473	2.9822	1.228	
1-A-41	1	CS	85.74	11.1	0.11	14C	1.4282	0.0555	6.0432	2.4921	1.226	
1-A-43	1	CS	89.83	12.5	0.25	14C-Anchor	0.6763	0.0319	5.7936	4.0642	1.225	
1-A-44	2	CS	93.53	15.2	0.50	Anchor	0.7145	0.0328	5.5485	3.6477	1.215	
1-A-44	2	CS	93.675	15.2	0.50	Anchor	0.7032	0.0314	5.3578	3.5261	1.208	
1-A-45	3	CC	96.7	16.0	0.60	Anchor	0.6601	0.0269	4.8134	3.0324	1.186	

1-A-46	3	CC	99.8	16.8	0.60	Anchor	0.8814	0.0344	4.9920	2.7403	1.192		
1-A-47	3	CC	102.8	18.3	0.65	Anchor	0.8459	0.0325	4.7186	2.5668	1.181		
1-A-48	2	CS	105.665	20.2	0.63	Anchor	0.8895	0.0386	4.9787	2.6745	1.190		
1-A-48	2	CS	105.818	20.3	0.63	Anchor	0.9174	0.0437	5.1023	2.7452	1.195		Artifact?
1-A-49	4	CC	108.9	22.4	0.82	Anchor	0.8223	0.0313	4.6899	2.4799	1.179		
1-A-51	4	CC	115.0	26.4	0.99	Anchor	0.8154	0.0309	4.5329	2.3614	1.173		
1-A-52	1	CS	117.01	27.7	0.94	Anchor	0.9723	0.0439	4.9278	2.3906	1.187		
1-A-52	4	CC	118.1	28.4	1.07	Anchor	1.2672	0.0501	5.4870	2.0118	1.203		
1-A-53	4	CC	121.1	30.5	1.16	Anchor	0.9685	0.0375	4.8440	2.2245	1.183		
1-A-54	4	CC	124.2	32.5	1.24	Anchor	0.9763	0.0369	4.9702	2.2738	1.188		
1-A-55	4	CC	127.2	34.5	1.32	Anchor	0.9375	0.0357	4.8667	2.3065	1.184		
1-A-56	4	CC	130.3	36.6	1.41	Anchor	0.8695	0.0332	4.6918	2.2784	1.178		
1-A-57	4	CC	133.3	38.6	1.49	Anchor	0.9127	0.0350	4.9116	2.3770	1.187		
1-A-58	4	CC	136.4	40.6	1.58	Anchor	0.9414	0.0469	5.0393	2.3706	1.191		
1-A-59	4	CC	139.4	42.6	1.66	Anchor	0.9710	0.0379	4.8814	2.2619	1.184		
1-A-60	2	CS	141.97	44.3	1.63	Anchor	1.1233		5.5927	2.4630	1.209		
1-A-60	4	CC	142.5	44.7	1.74	Anchor	0.8558	0.0345	4.4948	2.0531	1.170		
1-A-61	4	CC	145.5	46.7	1.84	Anchor	1.0832	0.0394	5.2884	2.3935	1.200		
1-A-62	4	CC	148.6	48.9	1.96	Anchor	0.9287	0.0396	4.8402	2.1759	1.183		
1-A-63	4	CC	151.6	51.1	2.08	Anchor	1.0720	0.0776	5.3601	2.4674	1.205		Br / Mg not conservative
1-A-65	3	CC	155.9	54.1	2.24	Anchor	1.1047	0.0413	5.5550	2.4533	1.208		
1-A-66	2	CS	158.11	55.7	2.23	Anchor	1.2544	0.0472	5.9545	2.5966	1.223		
1-A-66	2	CS	158.325	55.8	2.24	Anchor	1.2548	0.0504	5.9737	2.5811	1.224		Artifact?
1-A-67	4	CC	160.8	57.6	2.43	Anchor	1.1725	0.0411	5.8224	2.5624	1.218		
1-A-69	4	CC	166.9	61.9	2.67	Anchor	1.2068	0.0447	5.9549	2.5189	1.222		
1-A-70	4	CC	169.9	64.1	2.79	Anchor	0.9636	0.0486	5.9422	2.4076	1.218		>5% C.B.E
1-A-72	4	CC	176.0	68.4	3.02	Anchor	1.3685	0.0485	6.1631	2.3693	1.228		
1-A-73	1	CS	177.255	69.3	2.97	Anchor	1.4486		6.1703	2.3152	1.229		
1-A-74	4	CC	182.1	72.7	3.26	Anchor	1.3993	0.0498	6.1976	2.3040	1.228		
1-A-75	4	CC	185.2	74.9	3.38	Anchor	1.4544	0.0526	6.0587	2.1444	1.224		
1-A-77	1	CS	189.83	78.2	3.46	Anchor	1.5387	0.0732	6.1940	2.1448	1.229		Br / Mg not conservative
1-A-77	1	CS	190.245	78.5	3.48	Anchor	1.5557	0.0583	6.1960	2.1671	1.230		
1-A-78	4	CC	194.3	81.4	3.74	Anchor	1.4748	0.0531	6.0663	2.2145	1.225		
1-A-80	4	CC	200.4	85.7	3.97	Anchor	1.5738	0.0630	5.7541	1.9126	1.217		
1-A-81	3	CS	203.835	88.1	4.00	Anchor	1.7128	0.0669	6.3331	1.9442	1.234		
1-A-83	1	CC	209.6	92.2	4.33	Anchor	1.8268	0.0676	6.3975	1.5559	1.233		
1-A-86	4	CC	218.7	98.7	4.68	Anchor	1.4960	0.0617	6.0756	1.9465	1.226		
1-A-87	1	CS	220.545	100.0	4.65	Anchor	1.6144	0.0662	6.3565	2.0060	1.235		
1-A-87	1	CS	220.85	100.2	4.67	Anchor	1.6176	0.0679	6.3191	2.0110	1.235		
1-A-88	4	CC	224.8	103.1	4.92	Anchor	1.4594	0.0616	6.1292	1.9356	1.228		
1-A-90	3	CC	230.9	107.4	5.16	Anchor	1.5016	0.0637	6.2878	2.0341	1.234		
1-A-92	2	CC	235.3	116.7	3.09	Anchor	1.9338	0.0776	6.3450	1.2005	1.232		
1-A-91	2	CS	235.81	116.8	2.97	Anchor	1.7889	0.0928	6.4546	1.6990	1.237		Br / Mg not conservative

1-A-93	2	CC	237.3	116.9	3.01	Anchor	1.9054	0.0763	6.4192	1.3615	1.234	
1-A-95	3	CC	243.2	117.7	2.78	Anchor	2.0038	0.0751	6.3631	1.3056	1.233	
1-A-100	5	CC	256.2	119.3	2.27	Anchor	1.9233	0.0732	6.5004	1.3796	1.238	
1-A-101	3	CC	258.4	119.6	2.18	Anchor	1.5758	0.0688	6.3464	1.6464	1.235	
1-A-102	4	CC	261.4	119.9	2.07	Anchor	1.9973	0.0842	6.8553	1.3113	1.249	
1A-104	2	CS	266.99	120.6	1.75	Anchor	1.6544	0.0612	5.7987	2.1722	1.226	
1A-108	2	CS	279.494	122.2	1.26	Anchor	1.4128		5.8695	2.1076	1.215	
1-A-108	3	CC	279.7	122.2	1.35	Anchor	1.2603	0.0501	5.9398	2.5229	1.221	
1-A-109	3	CC	282.8	122.6	1.23	Anchor	1.3481	0.0488	6.0136	2.5490	1.225	
1-A-111	3	CC	288.9	123.8	1.10	Anchor	1.1416	0.0444	5.8255	2.6742	1.218	
1-A-116	3	CC	301.1	127.3	1.10	Anchor	1.5053	0.0559	6.0835	2.3356	1.224	
1-A-118	3	CC	305.9	128.7	1.10	Anchor	1.4688	0.0526	6.0119	2.2706	1.221	
1A-120	2	CS	309.04	129.6	1.00	Anchor	1.1885		5.8308	2.5925	1.221	
1-A-120	3	CC	309.9	129.8	1.10	Anchor	1.1433	0.0507	6.0304	2.5533	1.224	
1-A-122	4	CC	316.2	131.6	1.10	Anchor	0.8725	0.0413	5.8102	2.9760	1.221	
1-A-123	3	CC	318.8	132.4	1.10	Anchor	0.7982	0.0400	5.7146	3.2497	1.220	
1-A-126	3	CC	324.8	134.1	1.10	Anchor	0.8647	0.0375	5.7445	3.1418	1.221	
1-A-127	3	CC	327.4	134.8	1.10	Anchor	1.2137	0.0526	5.8350	2.4489	1.220	
1-A-129	2	CC	331.5	138.0	1.21	Anchor	1.0717	0.0463	5.9053	2.6152	1.221	
1-A-131	3	CC	337.6	143.1	1.40	Anchor	1.0104	0.0405	5.9590	2.8981	1.225	
1-A-132	4	CC	340.7	145.7	1.49	Anchor	0.9517	0.0382	5.8415	2.8708	1.221	
1-A-133	3	CC	343.7	148.3	1.58	Anchor	0.9809	0.0438	5.9357	2.7758	1.224	
1A-135	1	CS	347.82	151.8	1.61	Anchor	1.0203		5.8308	2.8159	1.222	
1-A-136	3	CC	352.9	156.0	1.87	Anchor	0.9243	0.0413	5.9342	2.8486	1.223	
1-A-137	3	CC	355.9	158.6	1.96	Anchor	0.9510	0.0426	5.7992	2.6736	1.218	
1-A-142	4	CC	370.5	171.0	2.41	Anchor	0.8367	0.0363	5.9632	3.0391	1.225	
1-A-146	3	CC	377.2	176.7	2.62	Anchor	0.8835	0.0426	5.9355	2.9104	1.224	
1-A-147	3	CC	380.3	179.2	2.71	Anchor	0.9669	0.0438	5.8105	2.8056	1.221	
1-A-149	3	CC	385.3	183.5	2.86	Anchor	1.1644	0.0488	5.8895	2.5076	1.223	
1-A-151	1	CC	390.4	187.8	3.02	Anchor	1.0790	0.0457	5.8737	2.5000	1.220	
1-A-153	3	CC	393.5	190.3	3.12	Anchor	1.1561	0.0519	5.9939	2.5163	1.227	
1-A-158	2	CC	404.7	195.7	3.48	Anchor	1.0135	0.0410	6.0985	2.5555	1.229	
1-A-164	4	CC	416.2	201.2	3.85	Anchor	1.2913	0.0554	6.0474	2.1045	1.225	
1-A-165	3	CC	419.2	202.7	3.95	Anchor	1.4182	0.0582	6.2164	2.0313	1.230	
1-A-167	3	CC	425.3	205.6	4.14	Anchor	0.9830	0.0588	6.3006	2.5988	1.236	Br / Mg not conservative
1-A-170	2	CC	431.4	208.6	4.34	Anchor	1.1326	0.0529	6.1469	2.4066	1.231	
1-A-172	3	CC	437.1	211.3	4.52	Anchor	1.0492	0.0526	5.8387	2.4076	1.222	
1-A-175	3	CC	443.6	214.5	4.73	Anchor	1.1223	0.0476	6.0287	2.8107	1.224	
1-A-176	3	CC	446.7	216.0	4.83	Anchor	0.7898	0.0400	5.7295	3.0073	1.217	
1-A-177	2	CC	446.9	216.1	4.84	Anchor	0.9185	0.0455	5.9541	2.9305	1.225	
1-A-178	2	CC	448.9	217.1	4.90	Anchor	0.9839	0.0466	5.7781	2.6958	1.218	
1-A-180	3	CC	450.7	217.9	4.96	Anchor	0.8949	0.0438	5.8717	2.8669	1.222	
1-A-181	2	CC	451.3	218.2	4.98	Anchor	1.0091	0.0466	5.8280	2.7359	1.220	

1-A-183	2	CC	452.9	219.0	5.03	Anchor	0.7976	0.0390	5.2328	2.6763	1.200	
1-A-185	2	CC	454.4	219.7	5.08	Anchor	1.0026	0.0479	5.8067	2.7699	1.221	
1-A-186	2	CC	455.0	220.0	5.10	Anchor	1.0080	0.0482	5.8401	2.7382	1.221	

Table DR 2: Phase analysis results. Correlation coefficients (r) for pore fluid records vs CO_2.

yrs	**Mg^{2+} vs. CO_2** (r)	**Br^- vs. CO_2** (r)
0	0.71	0.69
-1000	0.77	0.85
-2000	0.82	0.88
-3000	0.86	0.89
-4000	0.87	0.89
-5000	0.86	0.88
-6000	0.85	0.69

Table DR 3: The compiled age model dataset. A combination of radiocarbon dates (Neugebauer et al., 2014) and anchor age points (Torfstein et al., 2015). The bottom of the table (highlighted in grey) includes the radiocarbon dates not used in the compiled age model.

Depth (mblf)	**Age (ka)**			**Method**
0	0	±	0.2	
10.92	1.232	±	0.044	Radiocarbon
16.54	1.931	±	0.025	Radiocarbon
26.86	3.770	±	0.036	Radiocarbon
43.75	6.692	±	0.056	Radiocarbon
60.11	8.348	±	0.057	Radiocarbon
89.25	11.440	±	0.119	Radiocarbon
91.00	14.50	±	0.50	Anchor age
101.00	17.10	±	0.50	Anchor age
144.50	46.00	±	1.70	Anchor age
234.60	109.99	±	5.20	Anchor age
235.00	116.65	±	3.00	Anchor age
286.10	123.00	±	1.00	Anchor age
328.00	135.00	±	1.00	Anchor age
393.00	190.00	±	3.00	Anchor age
455.00	220.00	±	5.00	Anchor age
92.06	14.145	±	0.115	Radiocarbon
108.51	20.942	±	0.131	Radiocarbon
115.37	30.340	±	0.261	Radiocarbon
139.6	43.946	±	0.717	Radiocarbon
157.94	55.864	±	5.627	Radiocarbon